Supporting Information

Accurately Simulating Electrical Double Layers Structure and Formation Using All-atom Scaled-Charge Force Fields

Haoyu He[1], Jianguo Zhou[1], Lei Yang[1], Chenglin Liang[1], Shuaikai Xu[1], Ming Chen[2], Tangming Mo[1, *]

1 State Key Laboratory of Featured Metal Materials and Life-cycle Safety for Composite Structures, School of Mechanical Engineering, School of Physics Science and Technology, Guangxi University, Nanning, Guangxi 530004, China

2 State Key Laboratory of Coal Combustion, School of Energy and Power Engineering, Huazhong University of Science and Technology (HUST), 430074 Wuhan, China

* Email: motangming@gxu.edu.cn

Contents

Part S1. Parameters and properties of force fields

Table S1 Density, diffusion coefficient and ions volume for [EMIM][BF_4] of force fields at 400 K.

Force Field	Charge (e)	ρ (kg·m^{-3})	D_- ($\times10^{-11}$ m^2·s^{-1})	D_+ ($\times10^{-11}$ m^2·s^{-1})	Volume[b] (nm^3)	
					Cation	Anion
ANFF	1	1169.27	3.56	4.98	0.1190	0.0477
ASFF	0.8	1094.12	38.33	45.00	0.1190	0.0477
CGFF	0.78	1195.51	36.67	55.00	0.0654	0.0477
Exp[a]	—	1193.00	39.40	44.00	—	—

[a] Experimental data.[1]

[b] The volume of ions was calculated by the free volume method.[2]

Part S2. Calculation method of differential capacitance

The differential capacitance (C) of the EDLs is given by the following equation：

$$C = \frac{d\sigma}{d\varphi} \tag{1}$$

and the potential drop (φ) can be expressed as：

$$\varphi = (\varphi_{electrode} - \varphi_{bulk}) - (\varphi_{eletrode} - \varphi_{bulk})|_{\mathrm{PZC}} \tag{2}$$

where σ is the charge density of the electrode surface, $\varphi_{electrode}$ is the potential of the electrode, and φ_{bulk} is the potential of the bulk region. The electrode charge density *vs.* potential drop (σ-φ) curve can be obtained by a series of simulations conducted at various electrode potentials (**Fig. S1**). Then, the σ-φ curve is fitted using a fixed-order polynomial. Finally, the differential capacitance curve at the corresponding potential drop can be gained by the derivative of the polynomial.[3]

In this work, we initially employed a four-order polynomial to fit σ-φ curve using seventeen consecutive points, then evaluated the goodness of fit for each potential point against a predefined criterion (R^2=0.997). For certain potential points that deviated from the standard, we individually increased the order of the polynomial to ensure compliance. This method employs a different fitting order for each potential point, effectively minimizing the fitting error and enhancing the accuracy of the differential capacitance curve compared to the conventional approach. For example, our calculation method accurately shows an apparent minimum in the coarse-grained force field near the zero voltage, a feature distinct from the conventional calculation method (**Fig. S2a**). Also, the differential capacitance curves derived from conventional calculation methods exhibit variations in the goodness of fit at various potential points. This discrepancy could lead to some potential points deviating from theoretical expectations, thereby failing to represent the correct differential capacitance curves (**Fig. S2c**). It is noteworthy that employing different fitting criteria results in distinct differential capacitance curves (**Fig. S2a**). The greater the number of fitting points, the more potential points are discarded as a consequence, even though the goodness of fit is improved (**Fig. S2b**). The number of fitting points and the goodness of fit may be carefully balanced in light of the criteria.

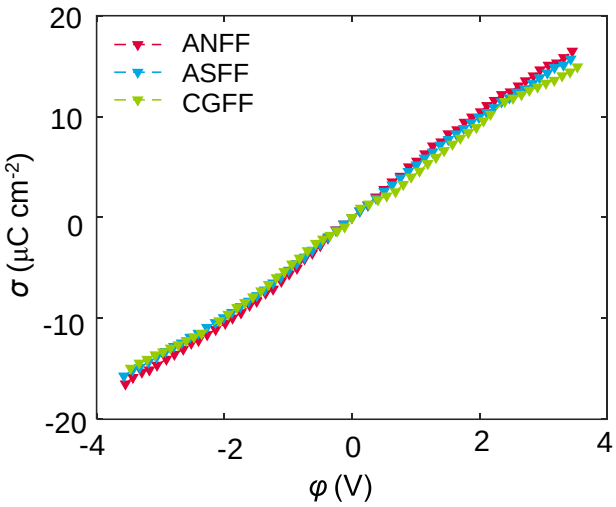

Figure S1. The relationship between surface charge density, σ, and the potential drop, φ.

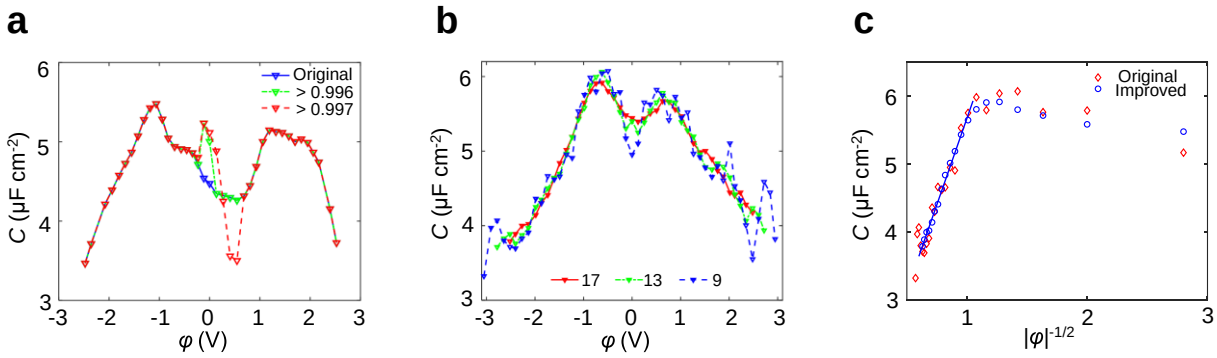

Figure S2. Capacitance *vs.* potential curves obtained using the different fitting methods. (**a**) Differential capacitance curves with different fitting criteria. (**b**) Multiple piecewise polynomials with 9,13, and 17 adjacent data points to fit the curve. (**c**) Traditional and improved differential capacitance calculations *vs.* mean-field theory.

Part S3. Charge storage of EDLs

Consistent with the electrode charge density, the differential capacitance of the all-atom force fields demonstrates a linear correlation with the inverse of the square root of the potential under high polarization (**Fig. S4a-b**). This finding aligns with the predictions in mean-field theory, revealing the variation of differential capacitance with $|C| \propto |\varphi|^{-1/2}$ under high polarization.[4] However, the coarse-grained force field (CGFF) is a significant deviation from theory predictions, with the capacitance not showing a correlation with the inverse of the square root of the potential (**Fig. S4c**).

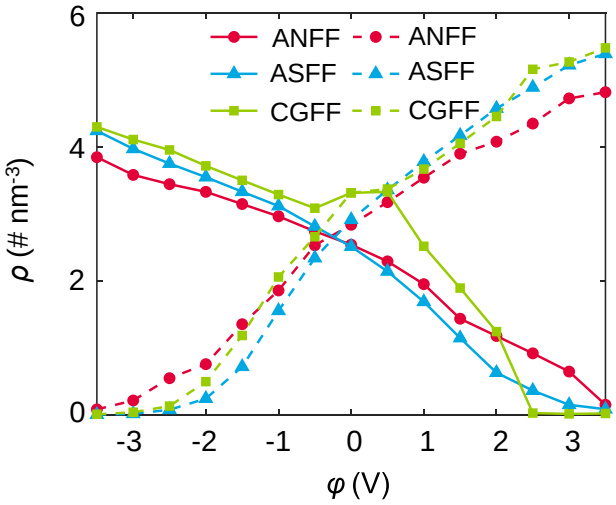

Figure S3. The number density of ions, ρ, under different EDLs potential drops, φ, where cations and anions are represented by solid and dashed lines, respectively.

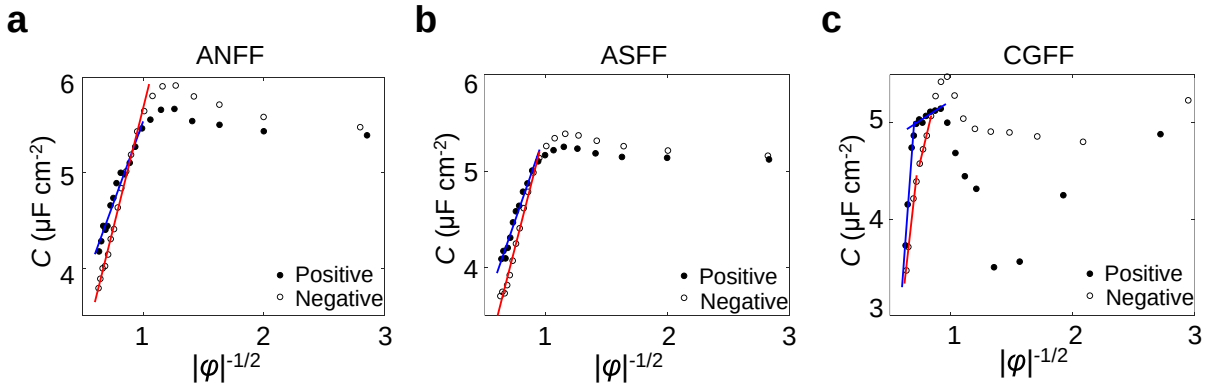

Figure S4. The relationship between the differential capacitance, C, and the inverse of the square root of the potential, $|\varphi|^{-1/2}$, for ANFF (**a**), ASFF (**b**), and CGFF (**c**). The red and the blue straight lines represent the fits to MD data in the high potential region.

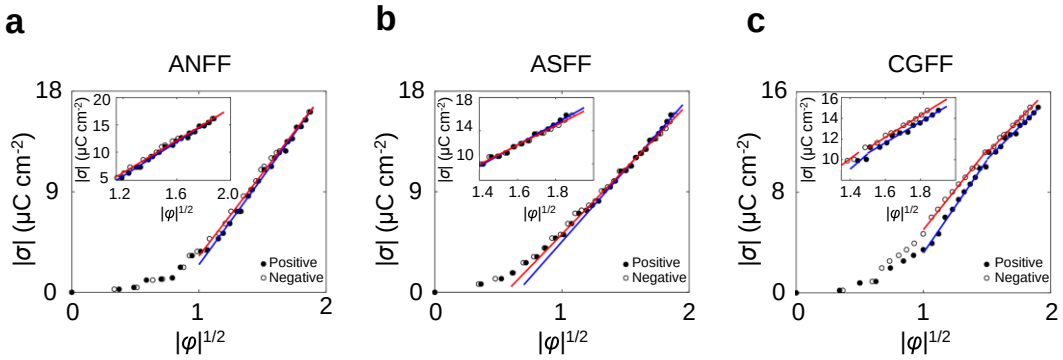

Figure S5. Structure of the EDLs at 298 K. (**a-c**) The relationship between the absolute value of electrode surface charge density, $|\sigma|$, and the square root potential, $|\varphi|^{1/2}$, for ANFF (**a**), ASFF (**b**), and CGFF (**c**). The red and the blue straight lines represent the fits to MD data in the high polarization region. The inset displays a local magnification of the high polarization region. (**d-f**) The number density of cations, ρ, as a function distance from the electrode surface, Z, for a series of potential across the EDLs, φ, for ANFF (**d**), ASFF (**e**), and CGFF (**f**), blue and orange in floor color correspond to negative and positive polarization respectively.

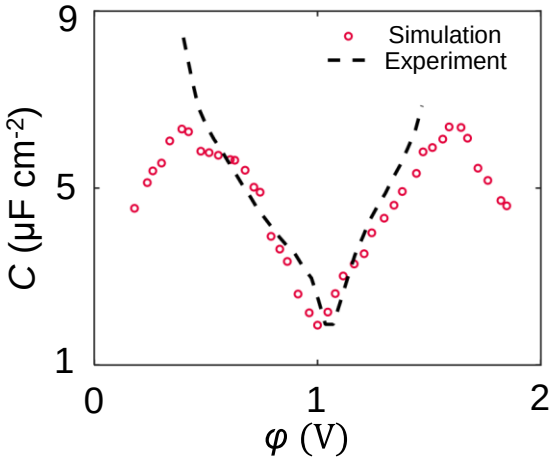

Figure S6. Differential capacitance curves in comparison with experiments[5] at 298 K.

Part S4. Overscreening phenomenon

As the positive polarization gets stronger, anions gradually accumulate until the electrode surface becomes completely occupied by anions (**Fig. S5a-c**). Anions in various force fields manifest a singular adsorption peak. Under weaker polarizations, the counterion groups nearest to the electrode surface provide higher values than the absolute charge density of the electrode, i.e., the overscreening phenomenon (**Fig. S5d-f**).[4]

The "effective ion accumulation" (EIA) factor was defined to further characterize the screening of the electrode by ions[6]:

$$EIA(z) = \frac{\int_0^z [\rho^n_{counter-ion}(s) - \rho^n_{co-ion}(s)]ds}{|\sigma|/_e} \quad (3)$$

where z is the distance from the electrode surface, e is the unit charge, and $\rho^n_{counter-ion}$ and ρ^n_{co-ion} are the number density of the counterion and the co-ion, respectively. The formation of an anionic layer leads to the accumulation of adjacent cations, forming alternating anionic and cationic layers and progressively weaker layers (**Fig. S6a**).

Taking the all-atom non-polarizable force field (ANFF) as an example (Left side of **Fig. S6b**), the EIA rapidly reaches 1.0 at z = 0.355 nm, signifying the precise screening of the electrode charge. Commencing at z = 0.465 nm, the EIA decreases rapidly with increasing distance. This indicates that the occurrence of the overscreening phenomenon in the region 0.355 nm < z < 0.465 nm. As the distance from the electrode increases, the charge of the excess anion is gradually neutralized by the charge of the cation. When the distance reaches z = 0.615 nm, the charge of the excess anions is balanced by the cations, exactly screening the electrode charge once again. With a further increase in distance from the electrode, the EIA decreases and eventually approaches zero at z = 0.685 nm, showing that the electrode is hardly screened. When z > 0.685 nm, the similar EIA curve reappears, with its amplitude diminishing as the distance from the electrode increases until the EIA attains 1.0. Analyses for the other force fields are similar (Middle and right side of **Fig. S6b**).

While the various force fields exhibit similar trends in the EIA curve, the magnitude of the EIA factor (overscreening strength) differs. The EIA curve in the CGFF demonstrates greater oscillations compared to the all-atom force field, both in the first adsorption layer and away from the electrodes (**Fig. S6b**). This phenomenon arises from the presence of a ring structure and a long alkyl chain in cation $[EMIM]^+$, promoting the cation closely to pack on the flat graphene electrode

surface and resulting in a strong attraction to the electrode. In contrast, these configurations are lacking in the cations of the coarse-grained model. Hence, the specific adsorption in the CGFF is absent, and interleaving takes place at the first anionic and the first cationic peaks, resulting in the anions undergoing neutralization by fewer cations. This enhances the ability of anions to screen the electrode surface charge. Therefore, the overscreening strength of the CGFF is overestimated.

Analogous to the behavior of cations on the negative electrode, the image charge induced by the anions of the ANFF on the electrode surface manifests more remarkable inhomogeneity than other force fields (Left side of **Fig. S6c**). Under weaker polarizations, some cations persist in the first adsorption layer without complete discharge, leading to more pronounced inhomogeneity compared to strong polarization. Owing to the strong Coulombic interactions in the ANFF, anions tend to cluster together at the electrode plate (Left side of **Fig. S6d**). The anions of the CGFF also show a "moiré-like" distribution (Right side of **Fig. S6d**).

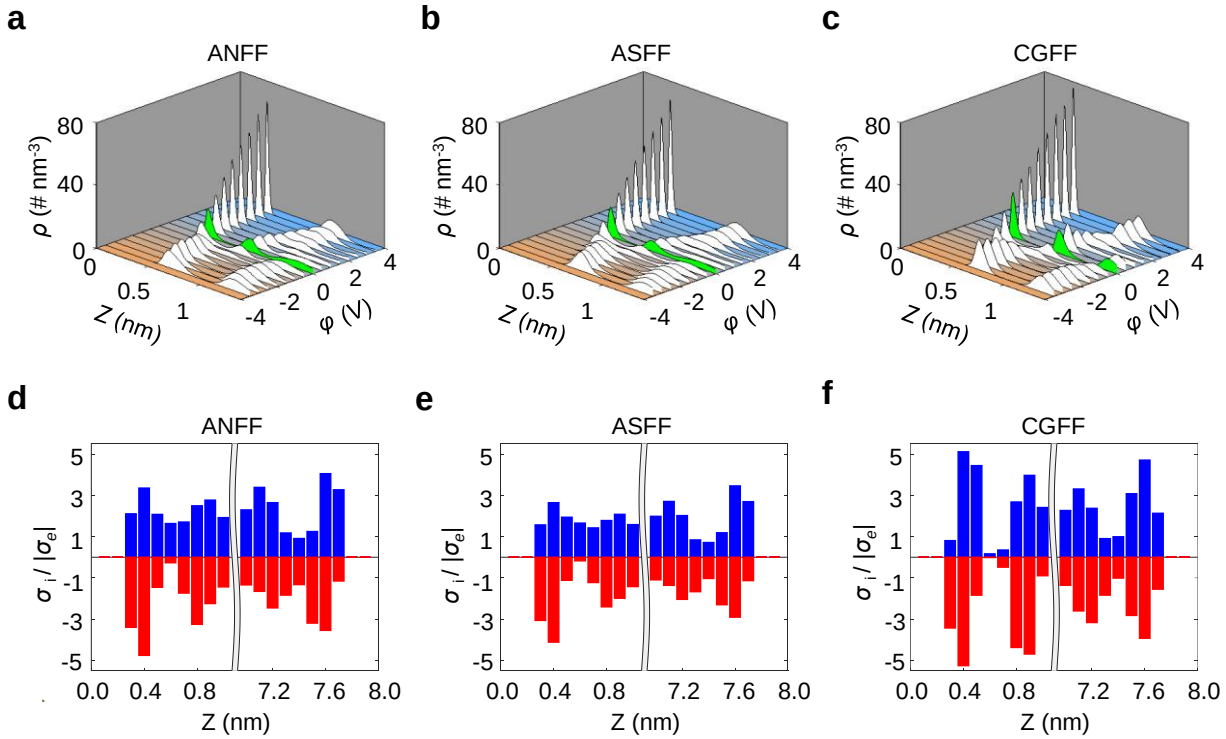

Figure S7. Overscreening phenomenon under weaker polarization. (**a-c**) The number density of anions, ρ, as a function distance from the electrode surface, Z, for a series of potentials across EDLs, φ, for ANFF (**a**), ASFF (**b**), and CGFF (**c**). Blue and orange in floor color correspond to positive and negative potential respectively. (**d-f**) Sliced average charge density per unit surface area, σ_i, scaled to the absolute value of the surface charge density of the electrode, $|\sigma_e|$, under a cell voltage of 1 V. ANFF (**d**), ASFF (**e**), and CGFF (**f**). The charge density per unit surface area was calculated for 0.1 nm thick slices. The anode and the cathode were separately placed at $Z = 0.1$ nm,

and Z = 7.8 nm. Blue bars correspond to cations, and red bars to anions.

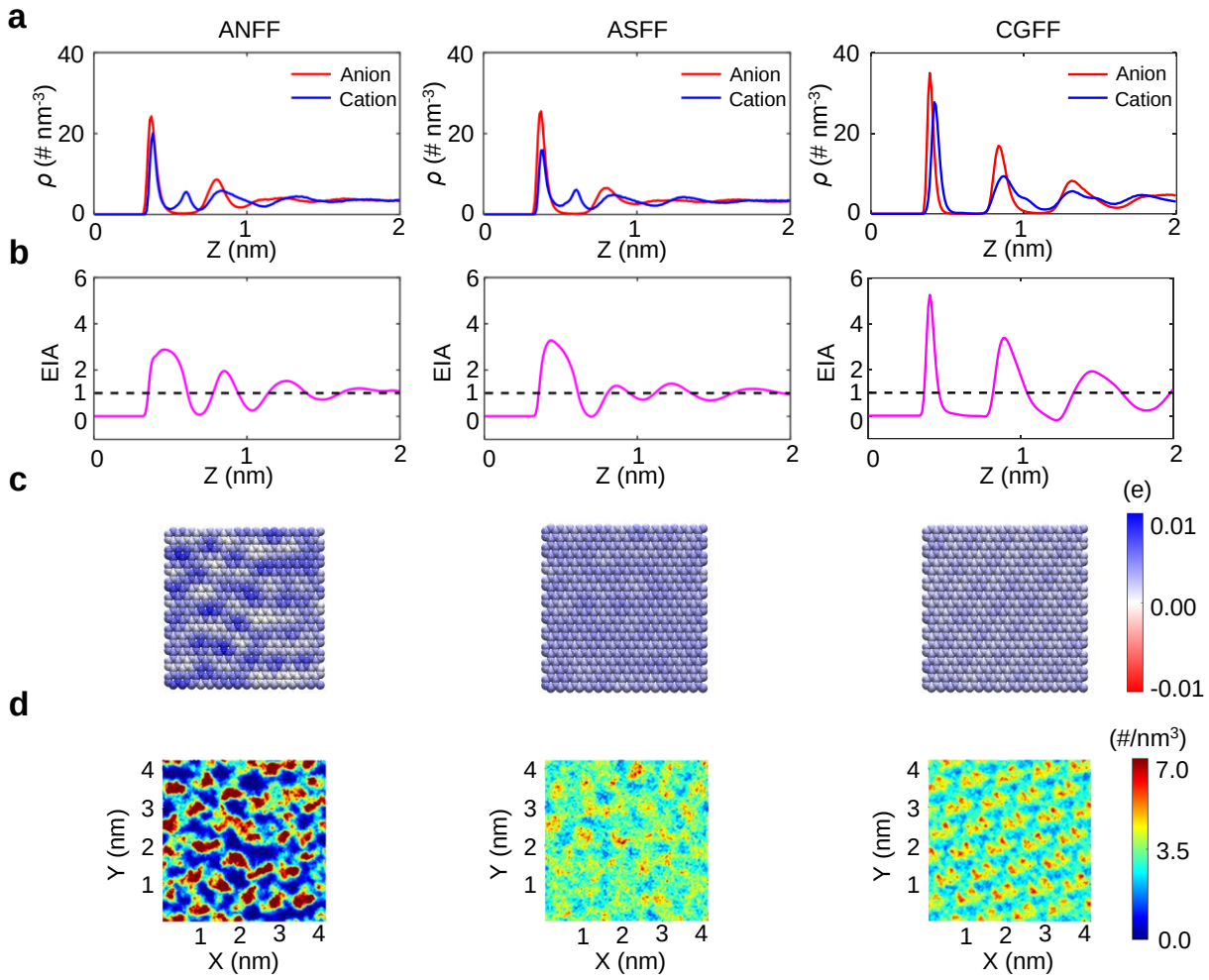

Figure S8. Overscreening strength at a cell voltage of 1 V. (**a**) Number density profiles of ions. (**b**) The effective ion accumulation (EIA) factor. (**c**) Distribution of instantaneous charge of electrode atoms. (**d**) Two-dimensional number density profiles of anions.

Part S5. Ions distribution near the electrode plate under high polarization

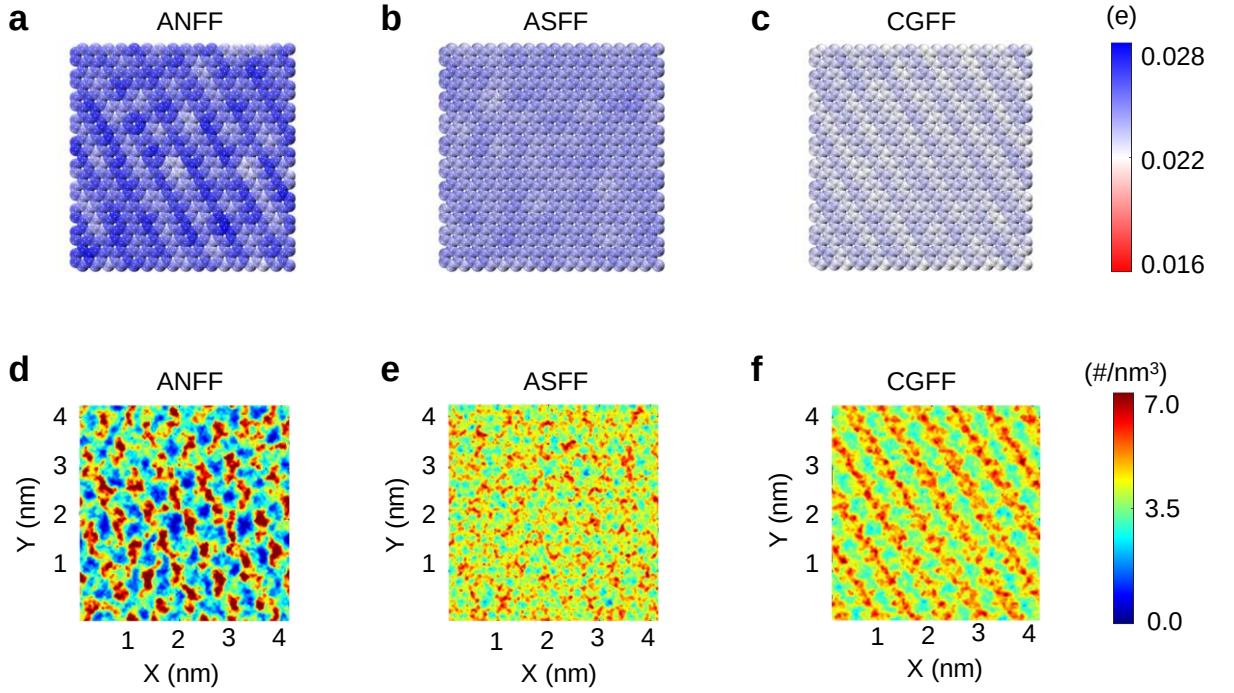

Figure S9. Distribution of anions near positive electrode plate. Distribution of instantaneous charge of electrode atoms for ANFF (**a**), ASFF (**b**), and CGFF (**c**). Two-dimensional number density profiles of anions for ANFF (**d**), ASFF (**e**), and CGFF (**f**).

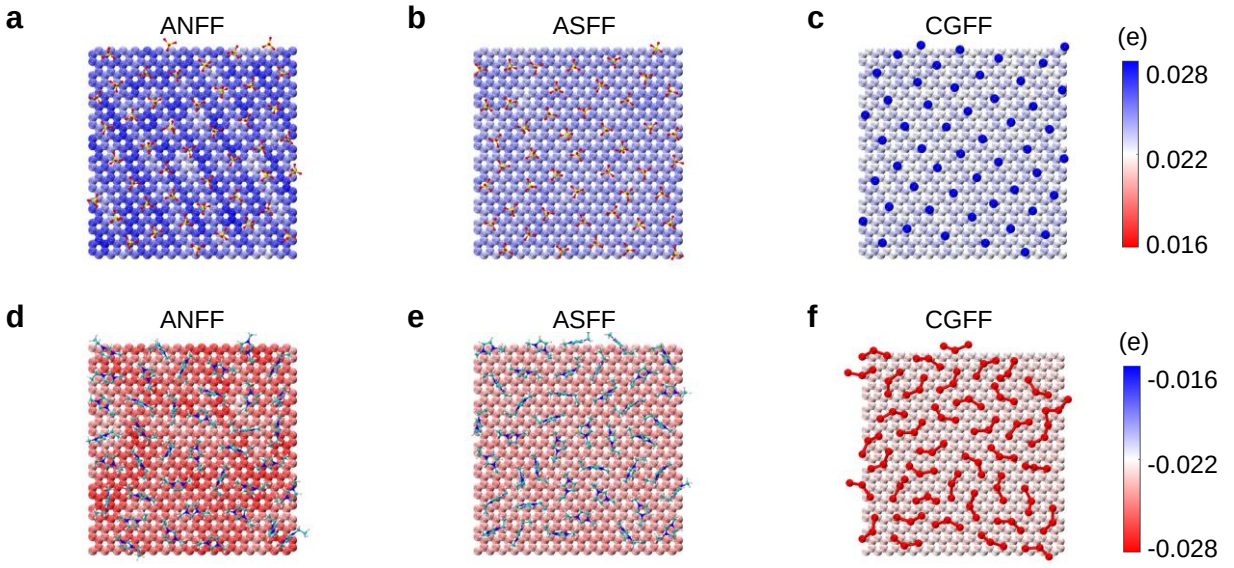

Figure S10. Arrangement of ions near the electrode plate. Arrangement of anions in the positive electrode plane for ANFF (**a**), ASFF (**b**), and CGFF (**c**). Arrangement of cations in the negative electrode plane for ANFF (**d**), ASFF (**e**), and CGFF (**f**).

References

1 C. Merlet, M. Salanne and B. Rotenberg, *J. Phys. Chem. C*, 2012, **116**, 7687–7693.

2 X.-Y. Wang, R. D. Raharjo, H. J. Lee, Y. Lu, B. D. Freeman and I. C. Sanchez, *J. Phys. Chem. B*, 2006, **110**, 12666–12672.

3 I. V. Voroshylova, H. Ers, V. Koverga, B. Docampo-Álvarez, P. Pikma, V. B. Ivaništšev and M. N. D. S. Cordeiro, *Electrochimi. Acta*, 2021, **379**, 138148.

4 M. Z. Bazant, B. D. Storey and A. A. Kornyshev, *Phys. Rev. Lett.*, 2011, **106**, 046102.

5 O. Oll, T. Romann, C. Siimenson and E. Lust, *Electrochem. Commun.*, 2017, **82**, 39–42.

6 G. Feng, J. Huang, B. G. Sumpter, V. Meunier and R. Qiao, *Phys. Chem. Chem. Phys.*, 2011, **13**, 14723.